

## Supporting Information

### **General Design of Self-Doped Small Molecules as Efficient Hole Extraction Materials for Polymer Solar Cells**

*Yuyuan Xue, Peipei Guo, Hin-Lap Yip, \* Yuan Li\* and Yong Cao*

# Table of contents

1. Materials and measurements .....	S3
2. Polymer solar cell device fabrication and characterization .....	S4
3. Hole only device fabrication .....	S5
4. Synthetic route for the phenolamine derivatives and TPA-OMe-DPP.....	S6
5. <sup>1</sup> H-NMR spectrum of TPA-OH <sub>2</sub> , TBP-OH <sub>4</sub> , TPD-OH <sub>4</sub> , Spiro-OH <sub>8</sub> and TPA-OMe-DPP .....	S9
6. UV-vis absorptions and PL spectra and solid powders images of all compounds.....	S14
7. <sup>1</sup> H NMR spectrum of TBP-OH <sub>4</sub> in CD <sub>3</sub> OCD <sub>3</sub> after adding [NO] <sup>+</sup> [PF <sub>6</sub> ] <sup>-</sup> .....	S15
8. Elemental and X-ray photoelectron spectroscopy (XPS) analysis.....	S16
9. Thin layer chromatography analysis for TPA-OH <sub>2</sub> , TBP-OH <sub>4</sub> , TPD-OH <sub>4</sub> and Spiro-OH <sub>8</sub> .....	S17
10. The enlarged <sup>1</sup> H NMR and ESR spectra of TPA-OMe-DPP .....	S18
11. Cyclic voltammograms curves of all compounds .....	S19
12. UV-vis-NIR spectra of oxidized species of TPA-OH <sub>2</sub> , TBP-OH <sub>4</sub> , TPD-OH <sub>4</sub> and Spiro-OH <sub>8</sub> .....	S22
13. Thermogravimetric analysis (TGA) and differential scanning calorimetry (DSC) curves of Spiro-OH <sub>8</sub> .....	S23
14. The ESR experiment of Spiro-OH <sub>8</sub> powder under UV-irradiation .....	S24
15. UV-vis absorption spectra of Spiro-OH <sub>8</sub> film and the water contact angle .....	S25
16. AFM height images of spin-coated Spiro-OH <sub>8</sub> on ITO .....	S26
17. The cross-linking SEM image of the PSC device .....	S27
18. <i>J-V</i> and EQE characteristics of devices with different spin-coating concentrations of Spiro-OH <sub>8</sub> as HTM.....	S28
19. The photovoltaic parameters of Spiro-OH <sub>8</sub> based polymer solar cells before and after 216 h storage in nitrogen protected glove box without encapsulation .....	S29

## 1. Materials and measurements

### Material

All the materials were purchased from commercial sources and used as received.

### Measurements

The  $^1\text{H-NMR}$  spectra of sample was recorded with a suitable amount of each sample dissolved in 0.5 mL of  $\text{CDCl}_3$ ,  $\text{CD}_3\text{COCD}_3$  and  $\text{DMSO-}d_6$  at room temperature by DRX-400 or 600 spectrometer (400 and 600 MHz  $^1\text{H-NMR}$  frequency, Bruker Co., Ettlingen, Germany). The UV-vis spectra were obtained by UV-3600 (Shimadzu Co., Japan). The fluorescence spectra were recorded by PL (FluoSENS, Gilden photonics Co., England). The thermal stability were investigated by thermogravimetric analysis (NETZSCH, STA449C) under protection of nitrogen at a heating rate of  $10\text{ }^\circ\text{C}/\text{min}$ . Differential scanning calorimetry (DSC) was recorded on a DSC201F2 differential scanning calorimeter under protection of nitrogen at a heating rate of  $10\text{ }^\circ\text{C}/\text{min}$ . Cyclic voltammetry (CV) was performed in  $\text{CH}_2\text{Cl}_2/\text{CH}_3\text{CN}$  ( $V_{\text{CH}_2\text{Cl}_2}/V_{\text{CH}_3\text{CN}}=12/1$ ) solution with 0.1 M tetrabutylammonium hexafluorophosphate ( $\text{Bu}_4\text{NPF}_6$ ) as the supporting electrolyte at a scan rate of 50 mV/s, a Ag/AgCl (3M KCl solution) electrode as the reference electrode, a carbon-glass electrode as the working electrode, a Pt line electrode as the counter electrode and ferrocene/ferrocenium ( $\text{Fc}/\text{Fc}^+$ ) as an internal reference on electrochemistry workstation (CHI660E, China). Electron spin resonance (ESR) spectra were measured on a Bruker ELEXSYS E500 spectrometer. Water contact angle was measured on a static contact angle tester (Dataphysics Co., German). The thicknesses of the films were obtained by the step profiler (Bruker Co., Ettlingen, Germany). The conductivities of samples were measured by the four-probe meter (Four-probe Co., Guangzhou, China). MALDI-TOF mass spectra (MS) were recorded on a Bruker Autoflex instrument using anthracene-1,8,9-triol as matrix. Elemental distribution on the surface of XPS spectra was analyzed on a Kratos Ultra Axis DLD spectrometer.

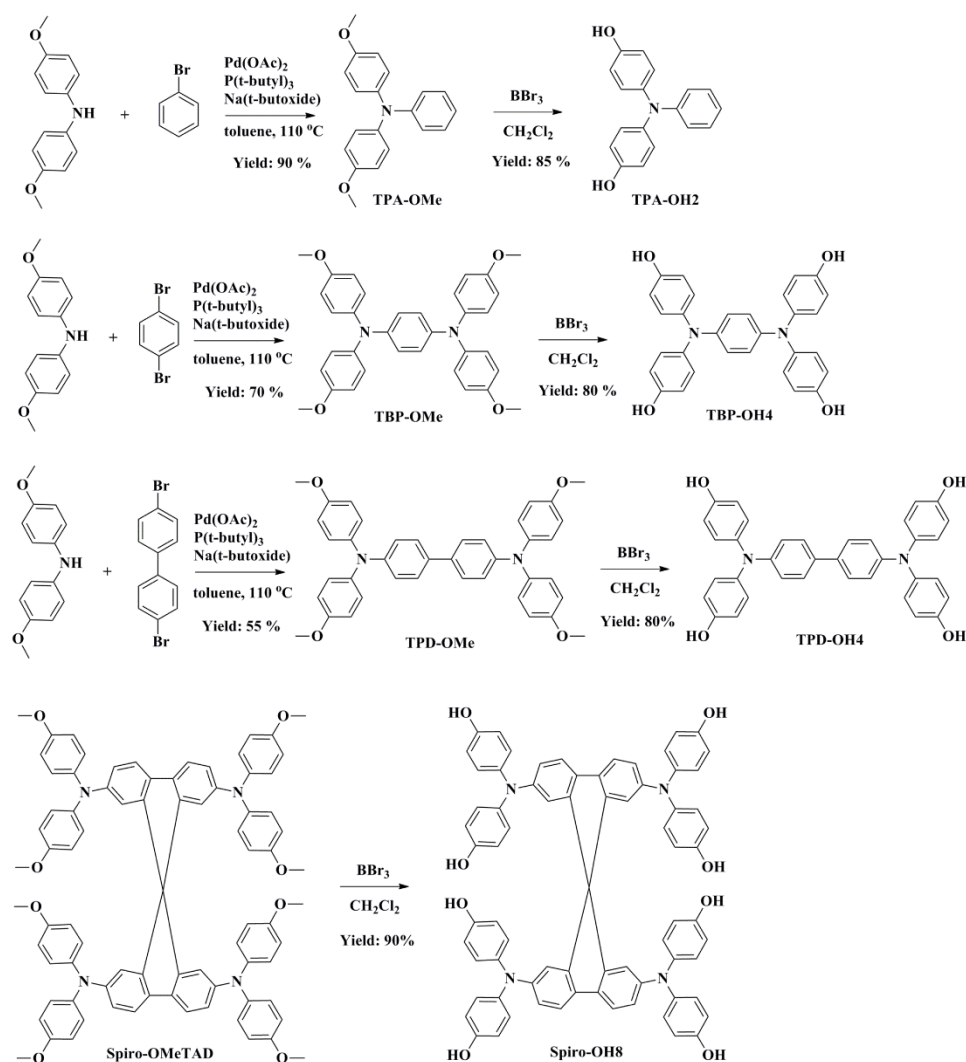
## 2. Polymer solar cell device fabrication and characterization

The ITO glass substrates were cleaned sequentially under sonication with acetone, detergent, deionized water and isopropyl alcohol and then dried in a baking oven overnight, followed by a plasma treatment. **Spiro-OH8** was prepared by dissolving in DMSO at a concentration of 5-16 mg/mL. **TPD-OH4** was prepared at a concentration of 5 mg/mL. The HEM was spun on ITO substrate (2000 rpm for 300 s; PEDOT:PSS at 3000 rpm for 30 s) and dried at 150 °C for 20 min in air. The blended solution was prepared by mixing PTB7-Th and PC<sub>71</sub>BM in a 1:1.5 weight ratio into chlorobenzene with the addition of a small amount of 1,8-Diiodooctane (DIO) (CB:DIO=100:3, v/v). The thickness of the PTB7-Th/PC<sub>71</sub>BM blended layers was ~100 nm. Preparation of the chlorobenzene solutions and subsequent spin coating of the solutions onto the HTM film was carried out in a N<sub>2</sub>-filled glove box. The PFN-Br dissolved in methanol at a concentration of 0.5 mg/ml was spun onto a PTB7-Th/PC<sub>71</sub>BM layer at 2000 rpm for 30 s. An aluminum electrode (80 nm) was finally deposited by thermal evaporation through a shadow mask under a base pressure of  $1 \times 10^{-7}$  mbar. The *J-V* curves of all devices were measured by a masking the active area with metal mask of 0.04 cm<sup>2</sup>. The device photocurrent was measured under an AM 1.5G solar simulator (Taiwan, Entelich). The current density-voltage (*J-V*) characteristics for the devices were recorded with a Keithley 2400 source meter. The illumination intensity of the light source was calibrated before testing using a standard silicon solar cell with a KG5 filter, calibrated using a National Renewable Energy Laboratory calibrated silicon photodiode, giving a value of 100 mW cm<sup>-2</sup> in the test.

### 3. Hole only device fabrication

The conductivity test of **Spiro-OH8** was conducted using space-charge-limited current (SCLC) method by testing *I-V* characteristics with hole-only device structure: ITO/**Spiro-OH8**/MoO<sub>3</sub> (5 nm)/Ag (100 nm). The patterned ITO glass substrates were cleaned using detergent solution, deionized water, acetone and alcohol in sequential ultrasonic baths and then dried at 120 °C in a vacuum oven for 20 minutes. **Spiro-OH8** layer was spin coated on the ITO substrate at 3000 rpm for 40 s with the concentration of 5 mg mL<sup>-1</sup> in DMF. Subsequently, MoO<sub>3</sub> layer was deposited on the layers of **Spiro-OH8**. Finally, 100 nm of Ag was deposited by thermal evaporation under a pressure of  $5 \times 10^{-4}$  Pa.

#### 4. Synthetic route for the phenolamine derivatives and TPA-OMe-DPP



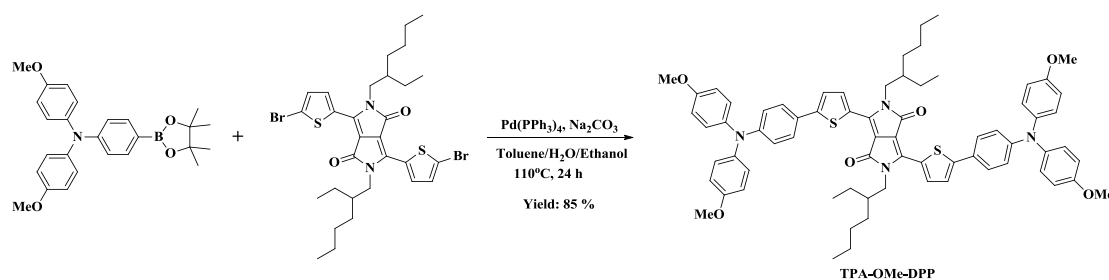
**Scheme S1.** Synthetic route for the phenolamine derivatives.

TPA-OMe, TBP-OMe and TPD-OMe were prepared according to literature procedure: 4,4'-dimethoxydiphenylamine (2.5 eq.), bromobenzene (2 eq.) or 1,4-dibromobenzene (1 eq.) or 4,4'-dibromobiphenyl (1 eq.), sodium tert-butoxide (4 eq.), palladium(II) acetate (0.01 eq.), tri-tert-butylphosphine (0.01 eq., added as a stock solution in toluene), and anhydrous toluene (25 mL) were added to a round-bottom flask. This solution was refluxed for 8 h under an argon atmosphere. After the mixture was cooled to room temperature, the organic layer was separated, dried over sodium sulfate, and evaporated to dryness. The crude product was purified by silica gel column chromatography with the mixed solution of dichloromethane and petroleum ether. Finally, the compounds were recrystallized from ethyl acetate: petroleum ether.

General procedure for **TPA-OH<sub>2</sub>**, **TBP-OH<sub>4</sub>**, **TPD-OH<sub>4</sub>** and **Spiro-OH<sub>8</sub>**: A solution of TPA-OMe, TBP-OMe, TPD-OMe or Spiro-OMeTAD (1 eq.) in dry  $\text{CH}_2\text{Cl}_2$  (20 mL) was cooled to  $-70^\circ\text{C}$  by ethanol and drikold, and

then  $\text{BBr}_3$  (10 eq.) was added dropwise under  $\text{N}_2$  over 5 min. After the cold bath was removed, the mixture was stirred at room temperature and under  $\text{N}_2$  for 1 day. Methanol (15 mL) was slowly added over 15 min and then the solvent was evaporated. After addition of water (40 mL) and ethyl acetate (50 mL), the crude product was extracted with ethyl acetate ( $2 \times 30$  mL). The mixtures were purified by column chromatography on silica gel with mixed solvents of ethyl acetate and petroleum ether. Finally, the compounds were recrystallized from ethyl acetate: hexamethylene in air.

### TPAOMe-DPP



### Scheme S2. Synthetic route for TPA-OMe-DPP.

TPA-OMe-DPP was prepared from 3,6-bis(5-bromothiophen-2-yl)-2,5-bis(2-ethylhexyl)-2,5-dihydropyrrolo[3,4-c]pyrrole-1,4-dione (1 eq.), 4-methoxy-N-(4-methoxyphenyl)-N-(4-(4,4,5,5-tetramethyl-1,3,2-dioxaborolan-2-yl)phenyl)aniline (2.5 eq.) and tetrakis(triphenylphosphine) palladium ( $\text{PPh}_3$ ) $_4$ Pd (0) (0.05 eq.) were dissolved in a mixture of degassed toluene (15 mL), Ethanol (5 mL) and  $\text{Na}_2\text{CO}_3$  (2M, 2 mL) in a 100 mL two-necked round bottomed flask under nitrogen atmosphere. The mixture was heated up to  $110^\circ\text{C}$  and kept for 24 h under nitrogen atmosphere. Upon reaction completion, the reaction mixture was poured into water and extracted with diethyl ether three times and dried with anhydrous  $\text{MgSO}_4$ . After concentration, the crude product was purified by silica gel column chromatography (eluted: ethyl acetate/hexanes = 1: 7 in volume) and then recrystallized from boiling diethyl ether to afford a brown solid (85 %).

$^1\text{H}$  NMR (400 MHz,  $\text{CDCl}_3$ ,  $\delta$ ): 8.98 (br, 2H), 7.45 (br, 4H), 7.32 (br, 2H), 7.11 (d,  $J = 8$  Hz, 8H), 6.93 (d,  $J = 8$  Hz, 4H), 6.86 (d,  $J = 8$  Hz, 8H), 4.06 (s, 4H), 3.82 (s, 12H), 1.96 (m, 2H), 1.41-1.27 (m, 16H), 0.91 (t,  $J = 8$  Hz, 6H), 0.86 (t,  $J = 8$  Hz, 6H). MALDI-TOF/MS ( $\text{M}^+$ ):  $m/z$  1130.330, calculated: 1130.505. Element analysis for  $\text{C}_{70}\text{H}_{74}\text{N}_4\text{O}_6\text{S}_2$ : calculated. C, 79.63; H, 8.19; N, 4.07; S, 5.67%; found C, 78.97; H, 9.78; N, 3.82; S, 5.39%.

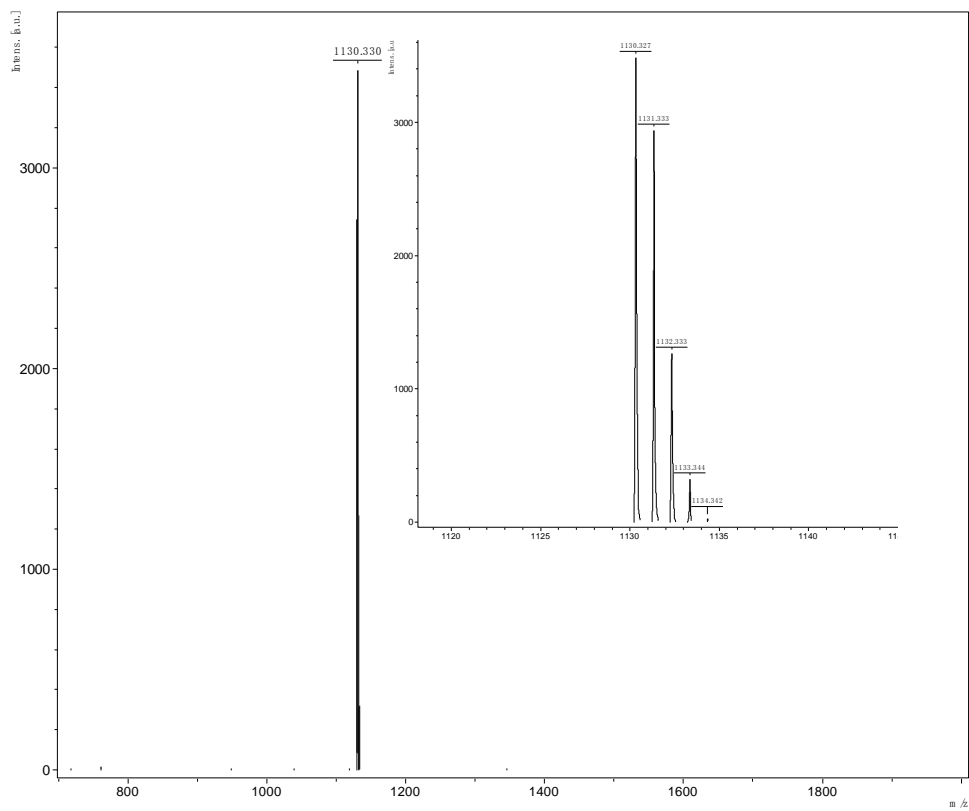


**Figure S1.** MALDI-TOF mass spectrum of TPA-OMe-DPP.

5.  $^1\text{H-NMR}$  spectrum of TPA-OH2, TBP-OH4, TPD-OH4, Spiro-OH8 and TPA-OMe-DPP

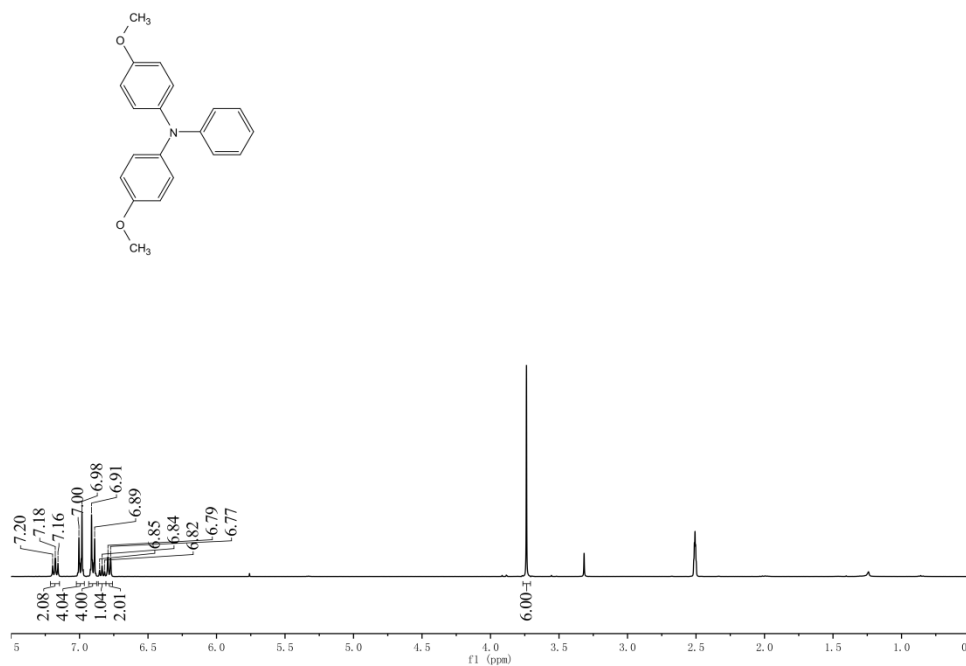


**Figure S2.**  $^1\text{H}$  NMR spectrum of TPA-OMe in  $\text{DMSO-}d_6$ .

**TPA-OMe** (Yield=90%):  $^1\text{H}$  NMR (400MHz,  $\text{DMSO-}d_6$ )  $\delta$  7.21-7.15 (t,  $J = 8$  Hz, 2H), 7.02-6.96 (m, 4H), 6.93-6.87 (m, 4H), 6.86-6.81 (t,  $J = 4$  Hz, 1H), 6.81-6.79 (d,  $J = 8$  Hz, 2H), 3.76-3.71 (s, 6H).

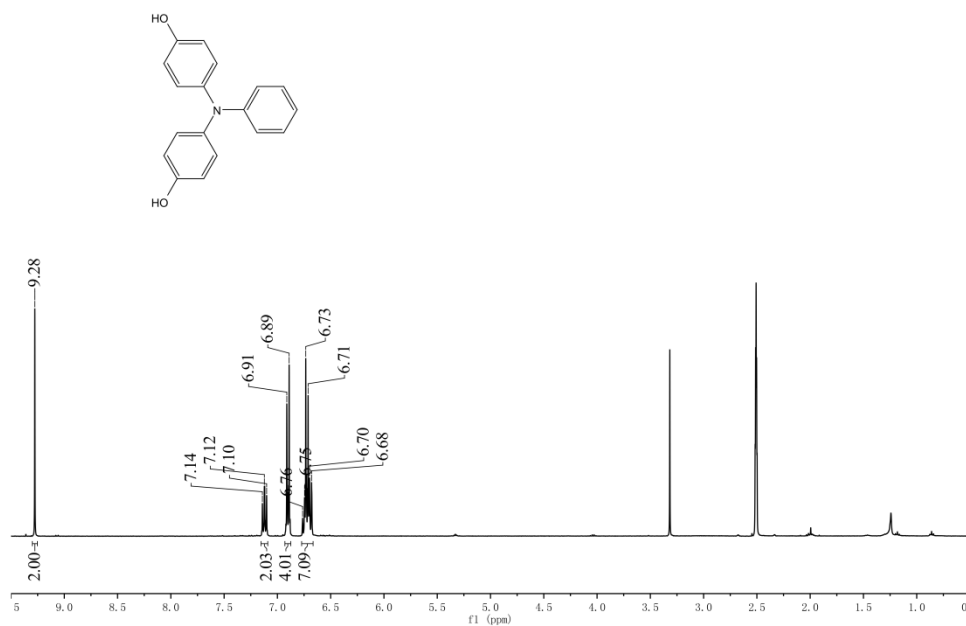


**Figure S3.**  $^1\text{H}$  NMR spectrum of TPA-OH2 in  $\text{DMSO-}d_6$ .

**TPA-OH2** (Yield=85%):  $^1\text{H NMR}$  (400MHz,  $\text{DMSO-}d_6$ )  $\delta$  9.30-9.25 (s, 2H), 7.15-7.09 (t, J=8 Hz, 2H), 6.93-6.88 (m, 4H), 6.77-6.67 (m, 7H). HRMS with electrospray ionization source (ESI) ion source calculated for  $\text{C}_{18}\text{H}_{16}\text{NO}_2$   $[\text{M}+\text{H}^+]^+$  278.1158, found 278.1176.

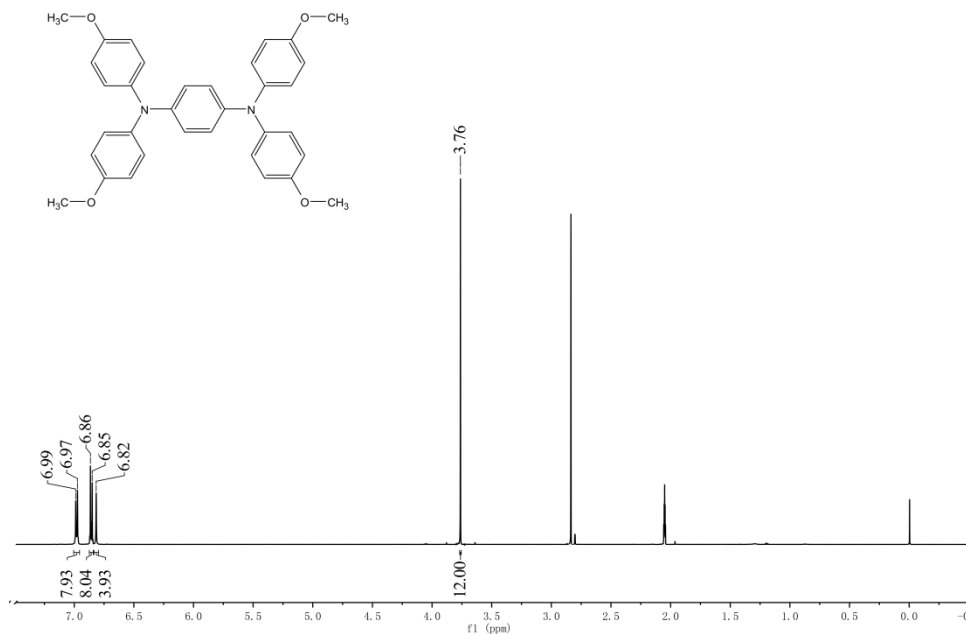


**Figure S4.**  $^1\text{H NMR}$  spectrum of **TBP-OMe** in  $\text{CD}_3\text{OCD}_3$ .

**TBP-OMe** (Yield=70%):  $^1\text{H NMR}$  (600MHz,  $\text{CD}_3\text{OCD}_3$ )  $\delta$  7.00-6.96 (m, 8H), 6.87-6.84 (m, 8H), 6.83-6.79 (br, 4H), 3.77-3.75 (s, 12H). HRMS with electrospray ionization source (ESI) ion source calculated for  $\text{C}_{34}\text{H}_{32}\text{NaN}_2\text{O}_4$   $[\text{M}+\text{Na}^+]^+$  555.2254, found 555.2249.

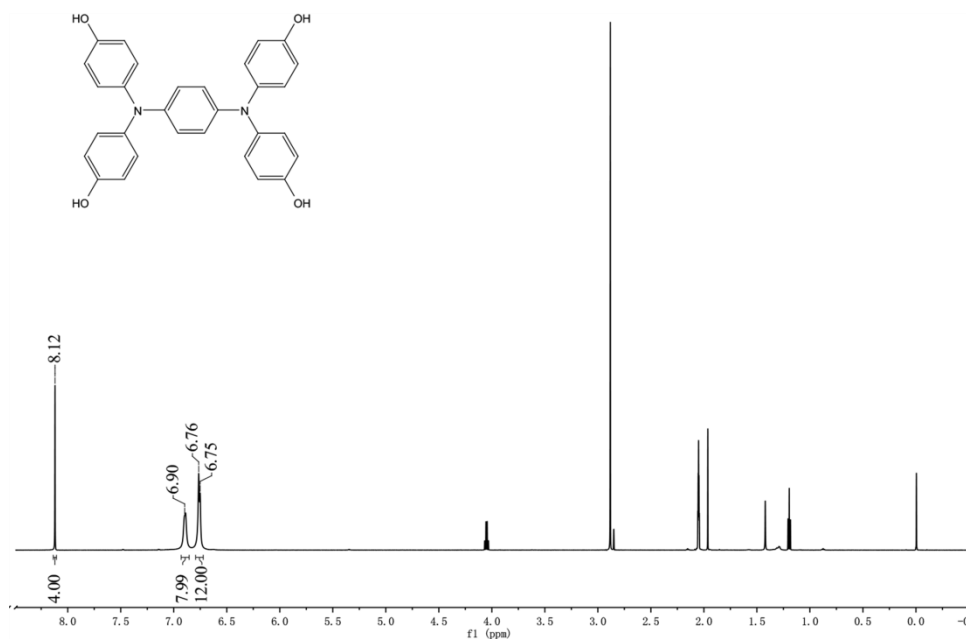


**Figure S5.**  $^1\text{H NMR}$  spectrum of **TBP-OH4** in  $\text{CD}_3\text{OCD}_3$ .

**TBP-OH4** (Yield=80%):  $^1\text{H NMR}$  (600MHz,  $\text{CD}_3\text{OCD}_3$ )  $\delta$  8.13-8.11 (s, 4H), 6.93-6.86 (br, 8H), 6.80-6.72 (br, 12H). HRMS with electrospray ionization source (ESI) ion source calculated for  $\text{C}_{30}\text{H}_{24}\text{NaN}_2\text{O}_4$   $[\text{M}+\text{Na}^+]^+$  499.1628, found 499.1613.

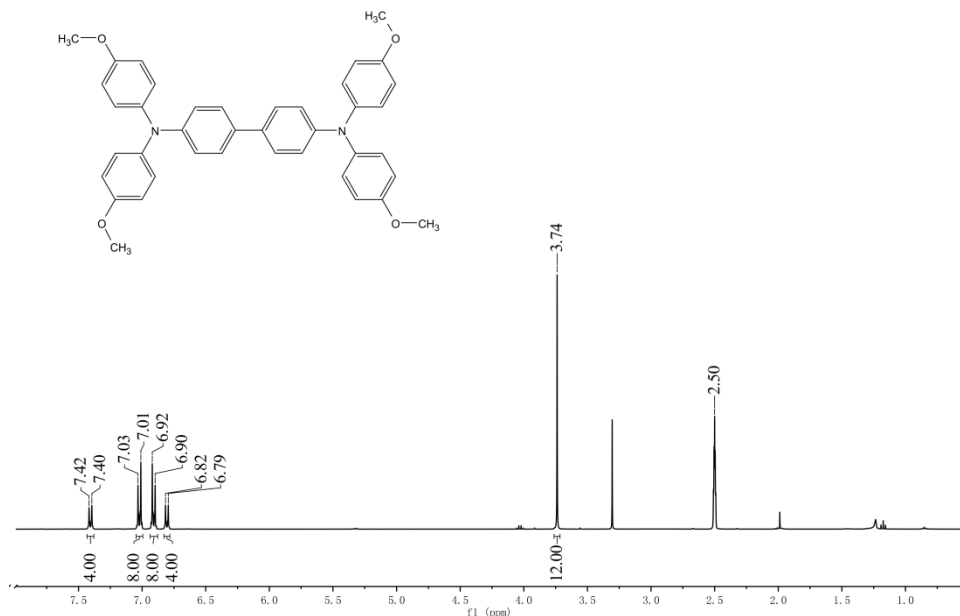


**Figure S6.**  $^1\text{H NMR}$  spectrum of **TPD-OMe** in  $\text{DMSO}-d_6$ .

**TPD-OMe** (Yield=55%):  $^1\text{H NMR}$  (400MHz,  $\text{DMSO}-d_6$ )  $\delta$  7.43-7.37 (d,  $J = 8$  Hz, 4H), 7.05-6.99 (d,  $J = 8$  Hz, 8H), 6.93-6.88 (d,  $J = 8$  Hz, 8H), 6.83-6.78 (d,  $J = 8$  Hz, 4H), 3.77-3.71 (s, 12H). HRMS with electrospray ionization source (ESI) ion source calculated for  $\text{C}_{40}\text{H}_{37}\text{N}_2\text{O}_4$   $[\text{M}+\text{H}^+]^+$  609.2748, found 609.2748.

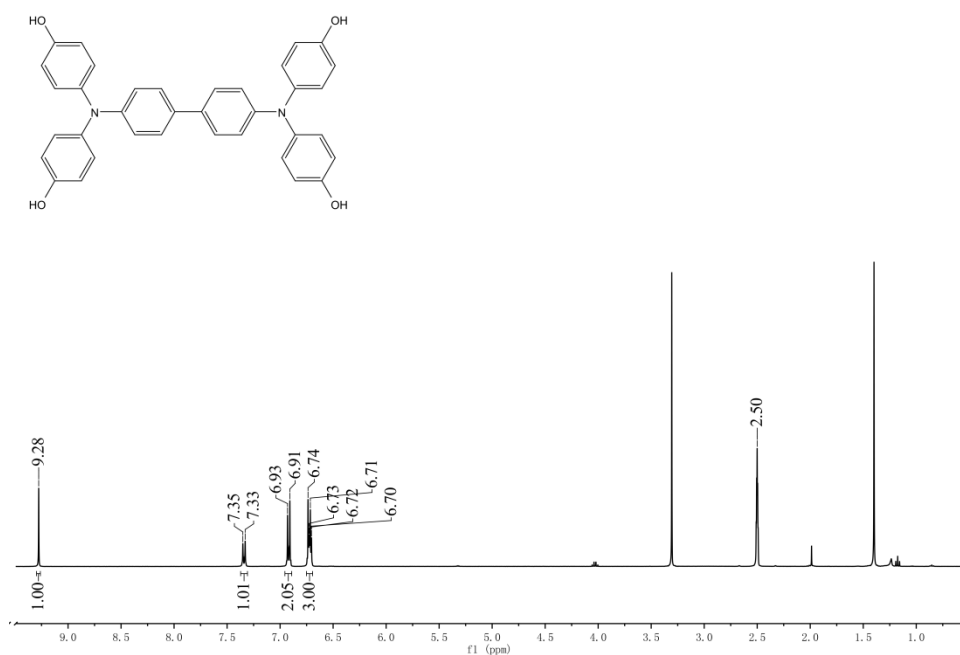


**Figure S7.**  $^1\text{H}$  NMR spectrum of **TPD-OH4** in  $\text{DMSO-}d_6$ .

**TPD-OH4** (Yield=80%):  $^1\text{H}$  NMR (400MHz,  $\text{DMSO-}d_6$ )  $\delta$  9.31-9.25 (s, 4H), 7.37-7.31 (d,  $J=8$  Hz, 4H), 6.95-6.89 (d,  $J=8$  Hz, 8H), 6.75-6.69 (m, 12H). HRMS with electrospray ionization source (ESI) ion source calculated for  $\text{C}_{36}\text{H}_{29}\text{N}_2\text{O}_4$   $[\text{M}+\text{H}^+]^+$  553.2122, found 553.2100.

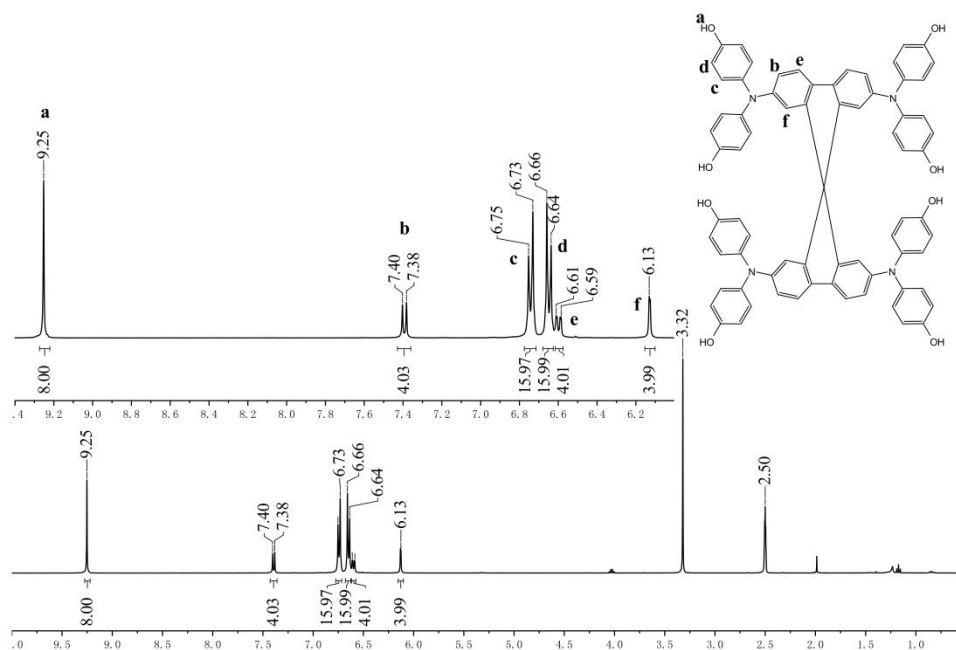


**Figure S8.**  $^1\text{H}$  NMR spectrum of **Spiro-OH8** in  $\text{DMSO-}d_6$ .

**Spiro-OH8** (Yield=90%):  $^1\text{H}$  NMR (600MHz,  $\text{DMSO-}d_6$ )  $\delta$  9.40-9.18 (s, 8H), 7.48-7.32 (d,  $J=12$  Hz, 4H), 6.83-6.70 (m, 16H), 6.68-6.61 (m, 16H), 6.61-6.57 (dd,  $J=1.8$ , 6 Hz, 4H), 6.20-6.06 (s, 4H). HRMS with electrospray ionization source (ESI) ion source calculated for  $\text{C}_{73}\text{H}_{52}\text{N}_4\text{NaO}_8$   $[\text{M}+\text{Na}^+]^+$  1135.3677, found 1135.3669.

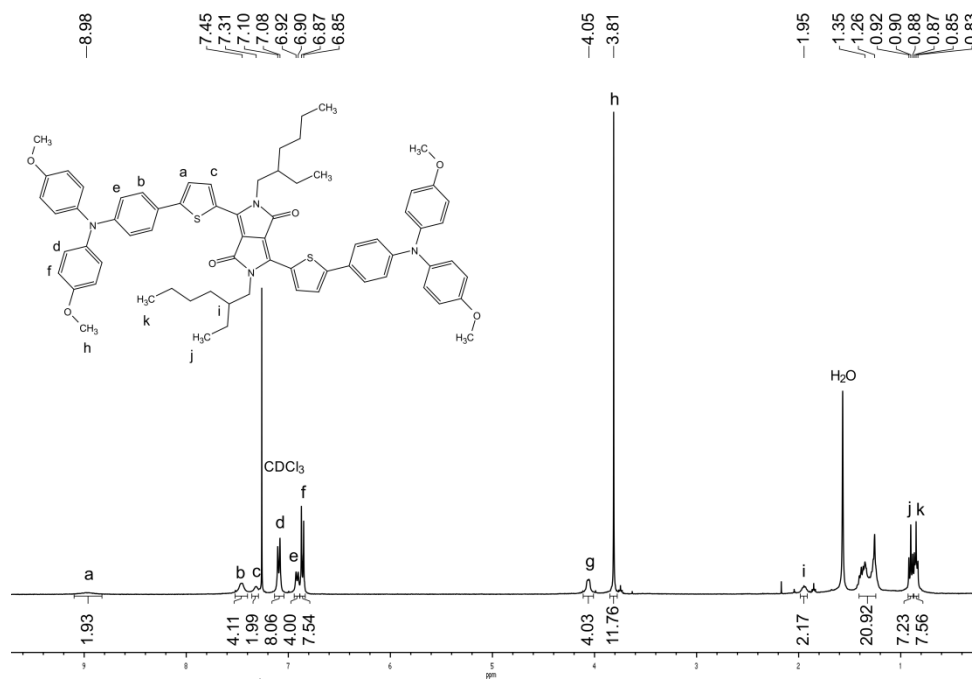


**Figure S9.** <sup>1</sup>H NMR spectrum of TPA-OMe-DPP in CDCl<sub>3</sub>.

## 6. UV-vis absorptions and PL spectra and solid powders images of all compounds

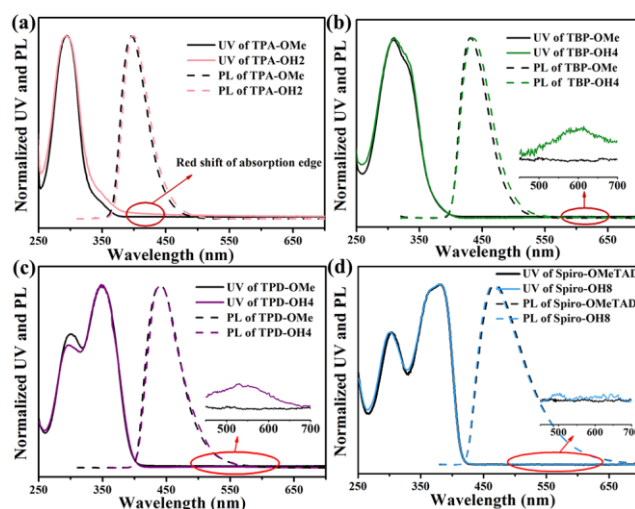


**Figure S10.** UV-vis absorptions and PL spectra of (a) TPA-OMe and **TPA-OH2**, (b) TBP-OMe and **TBP-OH4**, (c) TPD-OMe and **TPD-OH4**, (d) Spiro-OMeTAD and **Spiro-OH8**; Inset: enlarged spectra of UV-vis absorptions.



**Figure S11.** The image of solid powders of TPA-OMe, **TPA-OH2**, TBP-OMe, **TBP-OH4**, TPD-OMe, **TPD-OH4**, Spiro-OMeTAD and **Spiro-OH8**.

7.  $^1\text{H}$  NMR spectrum of TBP-OH4 in  $\text{CD}_3\text{OCD}_3$  after adding  $[\text{NO}]^+[\text{PF}_6]^-$

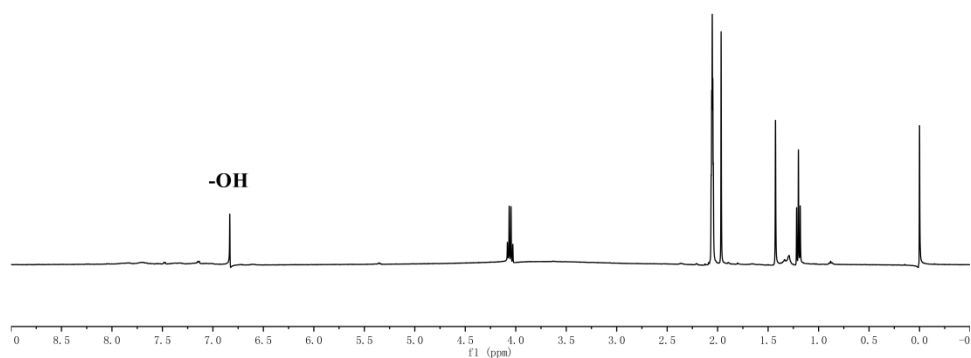


**Figure S12.**  $^1\text{H}$  NMR spectrum of **TBP-OH4** in  $\text{CD}_3\text{OCD}_3$  after adding  $[\text{NO}]^+[\text{PF}_6]^-$ .

## 8. Elemental and X-ray photoelectron spectroscopy (XPS) analysis of Spiro-OH8

**Table S1.** Elemental distribution of **Spiro-OH8** by elemental analysis method

Element	N%	C%	H% <sup>a</sup>	S%
Experimental result	5.22	74.13	5.38	0
Theoretical result	5.03	78.76	4.71	0

<sup>a</sup> Bound water is found in **Spiro-OH8** powder, which is in good agreement with TGA.

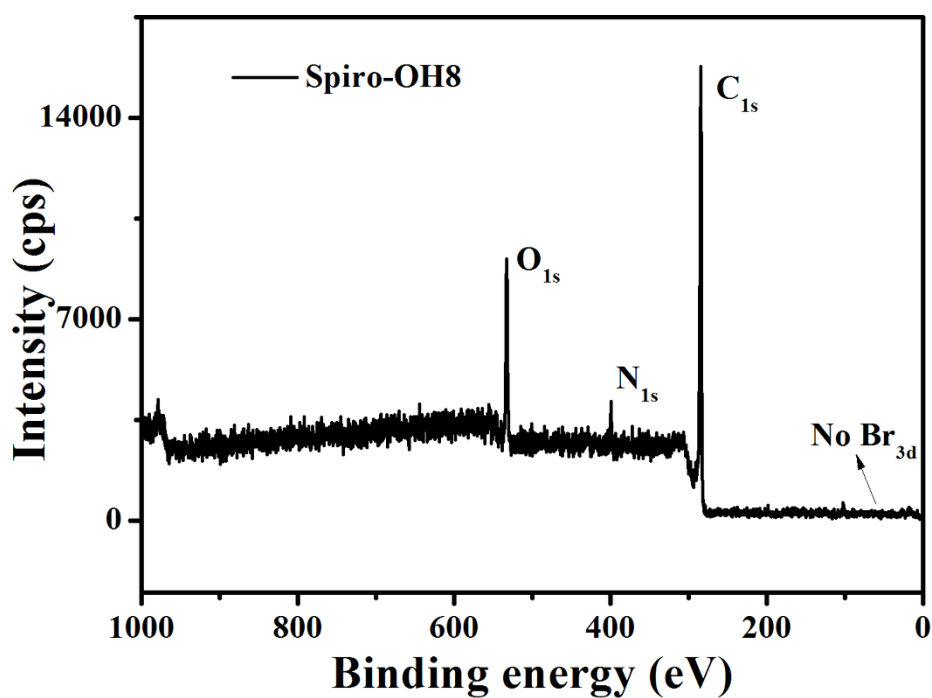


**Figure S13.** XPS spectrum of **Spiro-OH8**.

## 9. Thin layer chromatography analysis for Spiro-OH8.

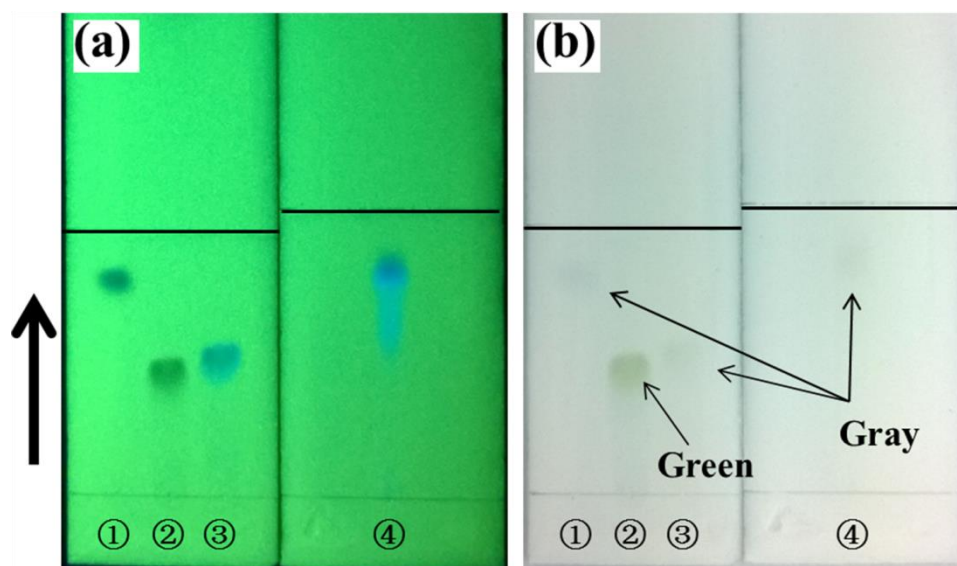


**Figure S14.** Photos of thin layer chromatography (TLC) analysis for **TPA-OH2 (1)**, **TBP-OH4 (2)**, **TPD-OH4 (3)** and **Spiro-OH8 (4)** under 253 nm (a) and room light (b) exposure; **TPA-OH2**, **TBP-OH4** and **TPD-OH4** was eluted with petroleum ether/ethyl acetate (1:1 in volume); **Spiro-OH8** was eluted with ethyl acetate (The photos were taken immediately after the elution process).

**TPA-OH2**, **TBP-OH4**, **TPD-OH4** and **Spiro-OH8** would be eluted with the mixed solutions of petroleum ether and ethyl acetate on the silica gel plate. Meanwhile, the products with deepened color could also be eluted in the thin layer chromatography (TLC) analysis, especially for **TBP-OH4**, owing to its obviously visible deep green color.

## 10. The enlarged $^1\text{H}$ NMR and ESR spectra of TPA-OMe-DPP

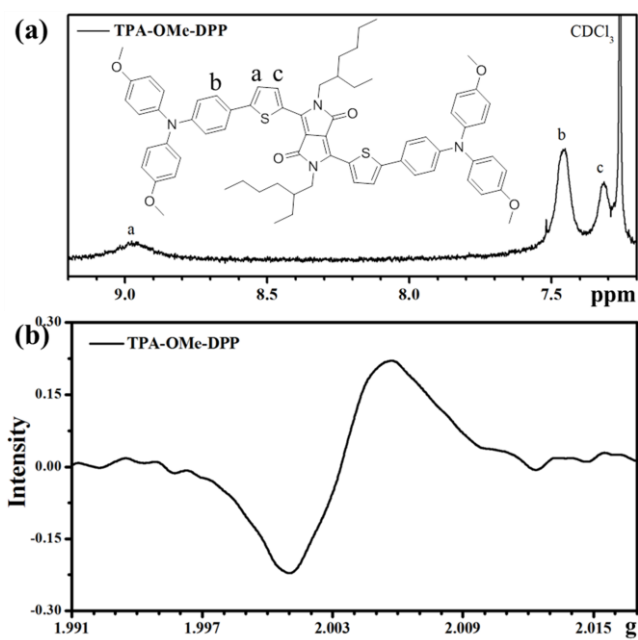


**Figure S15.** (a) The enlarged  $^1\text{H}$  NMR spectrum of TPA-OMe-DPP in  $\text{CDCl}_3$ . (b) ESR spectrum of TPA-OMe-DPP in powder form with 5 mg sample.

## 11. Cyclic voltammograms curves of all compounds

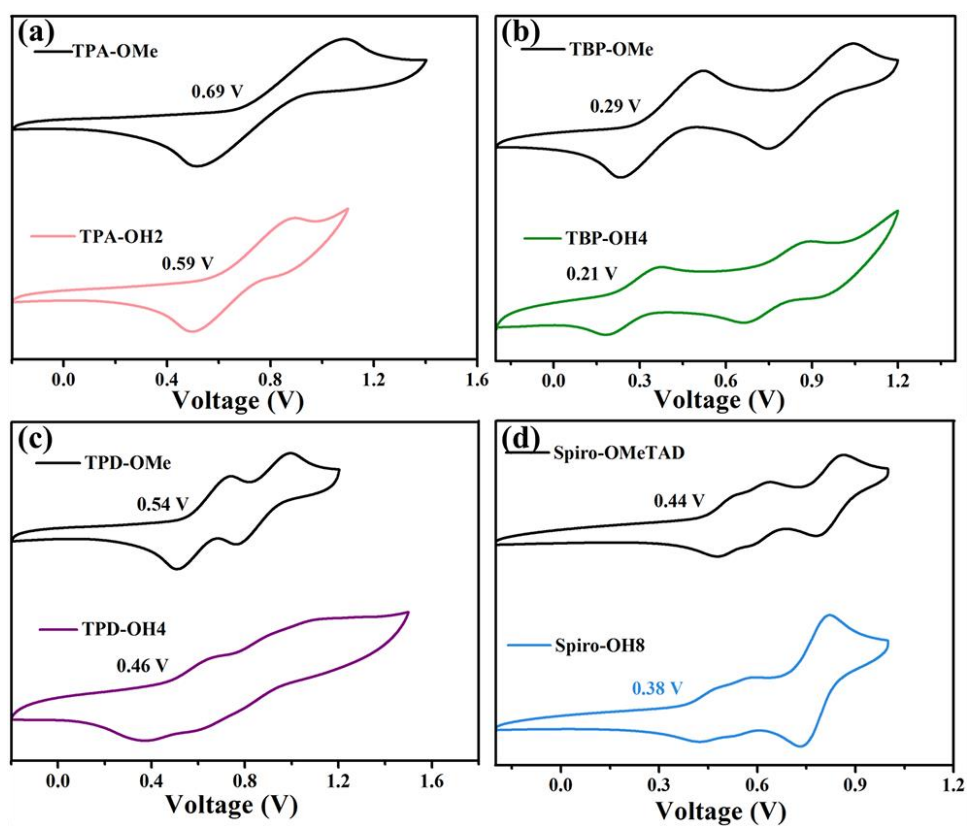


**Figure S16.** Cyclic voltammograms of (a) TPA-OMe and TPA-OH<sub>2</sub>, (b) TBP-OMe and TBP-OH<sub>4</sub>, (c) TPD-OMe and TPD-OH<sub>4</sub>, (d) Spiro-OMeTAD and Spiro-OH<sub>8</sub> in dichloromethane solution.

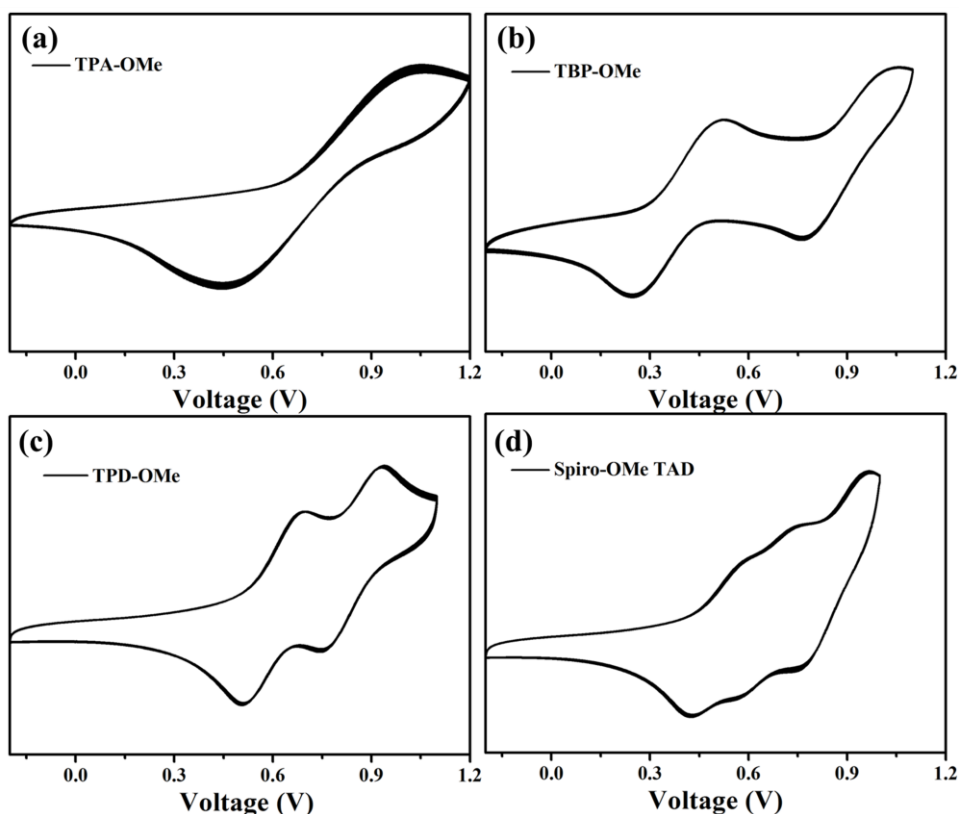


**Figure S17.** Electrochemical stability experiment of (a) TPA-OMe, (b) TBP-OMe, (c) TPD-OMe and (d) Spiro-OMe TAD at a scan rate of 50 mV/s.

The CV tests were performed to investigate the oxidation behaviors of the phenolamine derivatives to further understand the distribution of the spin densities on the nitrogen atoms (Figure 6). **TPA-OH2** exhibited one reversible oxidation wave with  $E_{ox}$  of 0.59 V, which can be correlated to the formation of triphenylamine (TPA) radical cation (Figure 6a). In contrast, **TBP-OH4** showed two reversible oxidation waves with  $E_{ox}$  of 0.21 V and 0.73 V, respectively, indicating that it can be reversibly oxidized into its radical cation and dication (Figure 6b). Analogously, **TPD-OH4** also displayed two reversible oxidation waves with  $E_{ox}$  of 0.46 V and 0.76 V, respectively (Figure 6c). The first two overlapped oxidation peaks of **Spiro-OH8** were attributed to the two consecutive oxidation reactions of the molecule when its radical monocation and quinoidal dication were generated, respectively. **Spiro-OH8** could be reversibly oxidized into radical cation, diradical dication and trication at  $E_{ox}$  of 0.38 V, 0.49 V and 0.71 V (Figure 6d). The planarity is closely related to the conjugate effect and electronic density. Oxidation potentials of **TPA-OH2**, **TPD-OH4**, **Spiro-OH8** and **TBP-OH4** were successively enhanced and the trend was consistent with the difference of planarity of the four compounds. Meanwhile, it was worthy to notice that the potential of two oxidation peaks of **TBP-OH4** are very different (0.21 V and 0.73 V, respectively). Such an improvement of oxidation potential can be explained by the stabilized monoradical of **TBP-OH4**. In addition, in spite of the relatively weak electron-donating effect of -OH than that

of -OMe, the change of the substitution from -OMe to -OH only resulted in a slight decrease of oxidation potential ranged from 0.06 V to 0.10 V.

12. UV-vis-NIR spectra of oxidized species of TPA-OH2, TBP-OH4, TPD-OH4 and Spiro-OH8

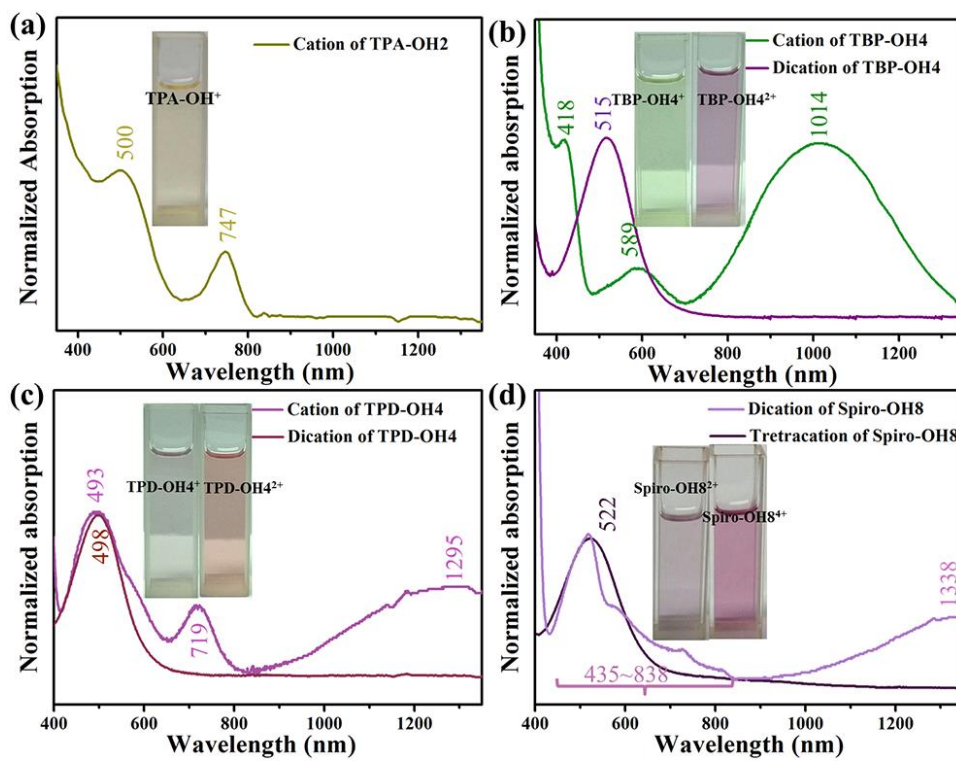


**Figure S18.** UV-vis-NIR spectra of oxidized species of TPA-OH2 (a), TBP-OH4 (b), TPD-OH4 (c) and Spiro-OH8 (d); Insert: the images of oxidized species of the four phenolamine derivatives in ethyl acetate.

### 13. TGA and DSC curves of Spiro-OH8

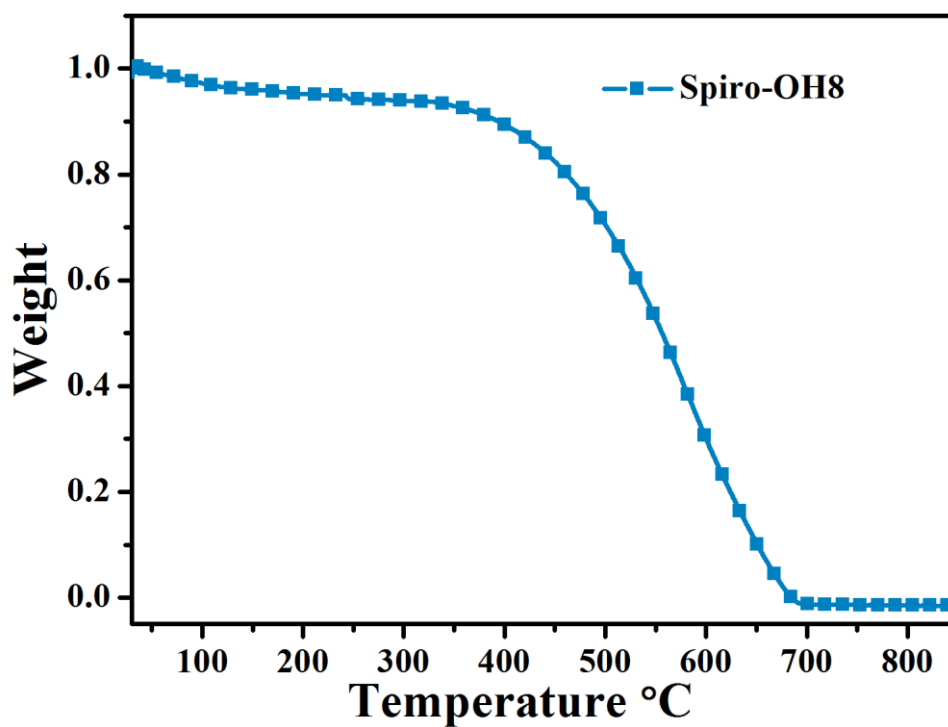


Figure S19. TGA curve of Spiro-OH8.

About ~10% bound water was found in TGA due to the hydrogen bonding effect of Spiro-OH8 with water.

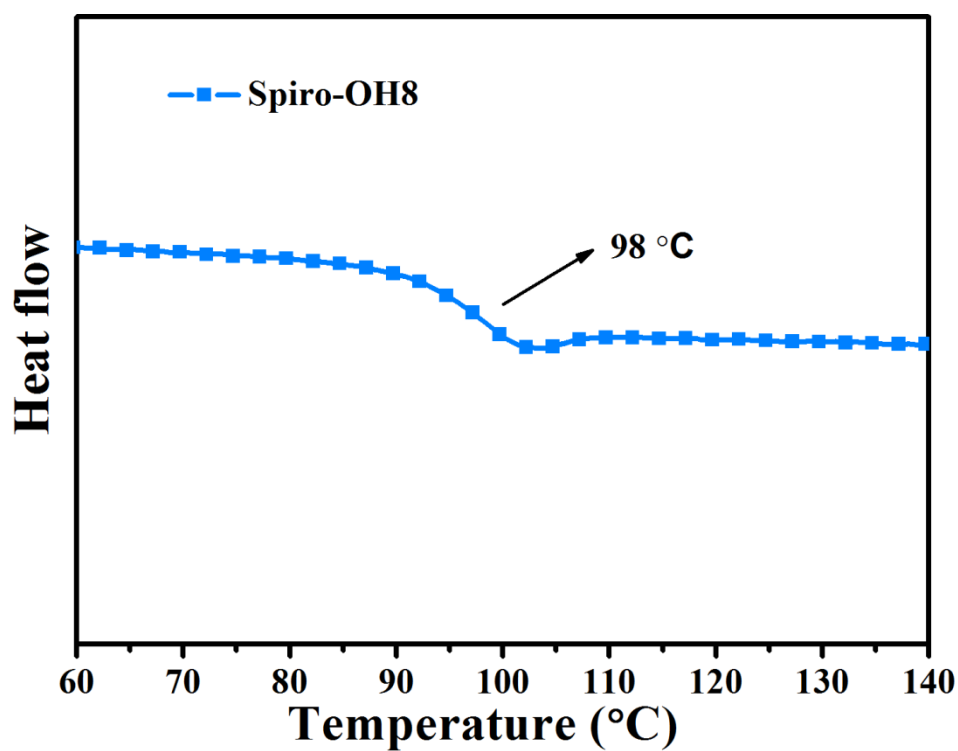
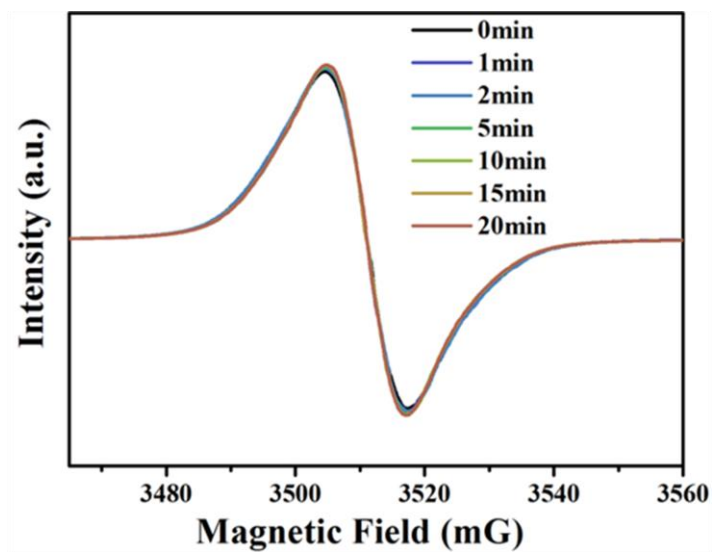


Figure S20. DSC curve of Spiro-OH8.

#### 14. The ESR experiment of Spiro-OH8 powder under UV-irradiation



**Figure S21.** The ESR experiment of Spiro-OH8 powder under UV-irradiation.

## 15. UV-vis absorption spectra of Spiro-OH8 film and the water contact angle

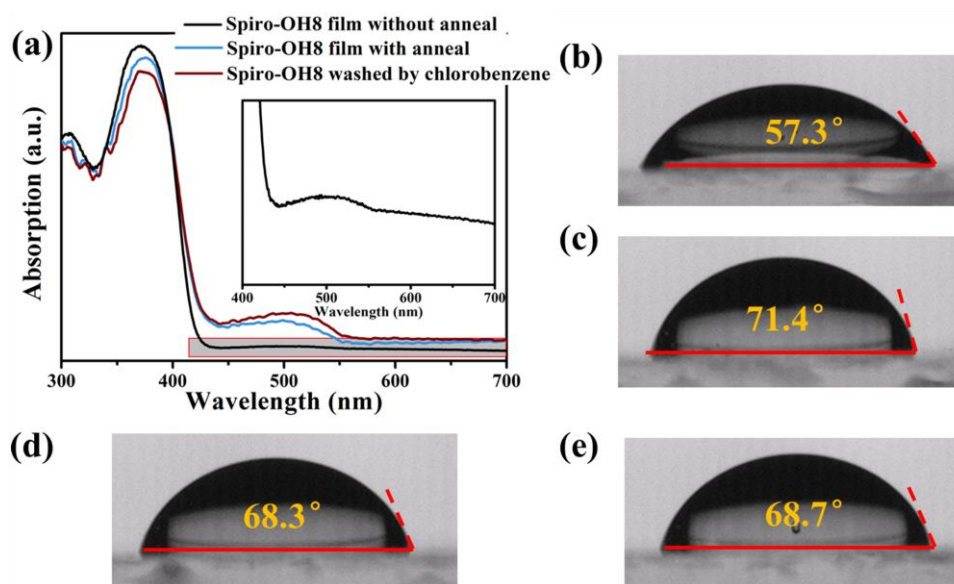


**Figure S22.** (a) UV-vis absorption spectra of Spiro-OH8 film on quartz (Anneal at 150 °C in air; without anneal; washing by chlorobenzene). The water contact angle for annealed film of (b) PEDOT: PSS-4083 (c) TBP-OH4 (d) TPD-OH4 and (e) Spiro-OH8, respectively.

The thin film UV-vis absorption of Spiro-OH8 was very useful for the characterization of anti-erosion and radical state in film form. Good solvent resistance of Spiro-OH8 against the processing solvent of the active layer is an important criterion for fabricating robust multilayers devices. In order to evaluate the resistance of Spiro-OH8 to chlorobenzene solvent, the absorption spectra of Spiro-OH8 film before and after spin-casting of pure chlorobenzene were compared and there was no obvious change in absorbance at 301 nm, indicating that Spiro-OH8 were robust enough for solution-processed PSCs. The weak absorption changes at 380 nm and 515 nm ascribed to the resonance structure transformation to radical structure, when the pure chlorobenzene was spin-casting on the Spiro-OH8 film.

## 16. AFM height images of spin-coated Spiro-OH8 on ITO

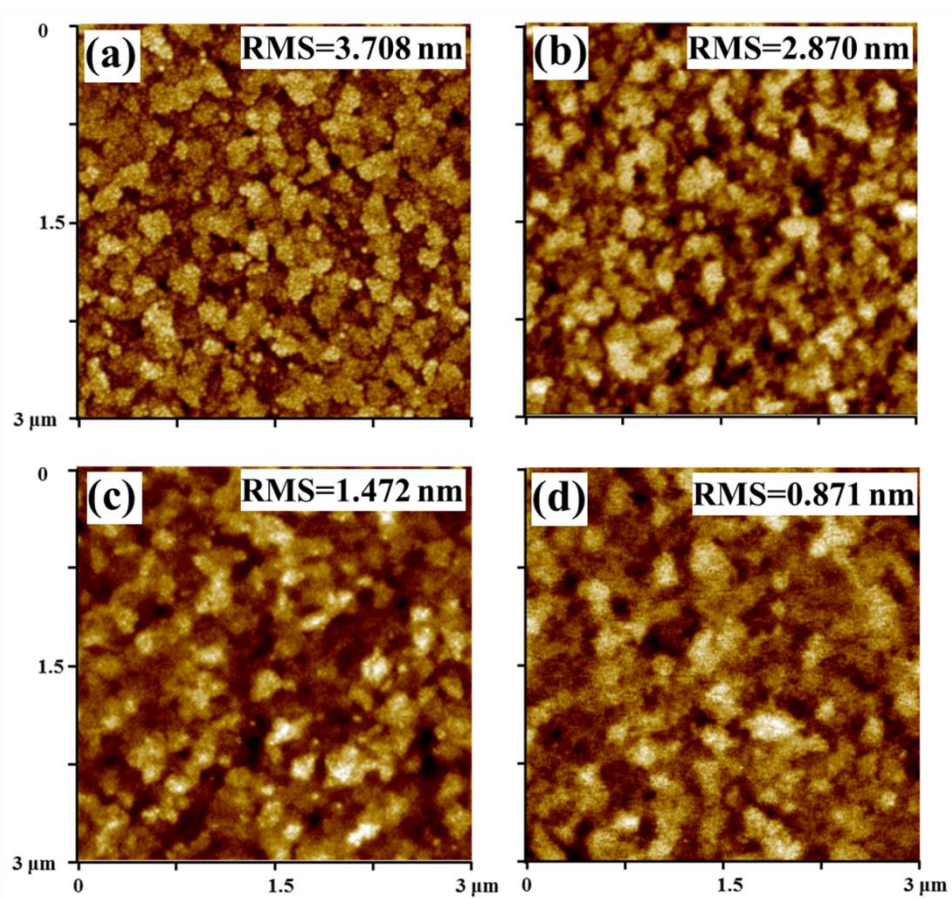


**Figure S23.** AFM height images of spin-coated **Spiro-OH8** on ITO with different concentration: (a) 0 mg/mL, (b) 5 mg/mL, (c) 10 mg/mL and (d) 16 mg/mL.

**17. The cross-linking SEM image of the PSC device**

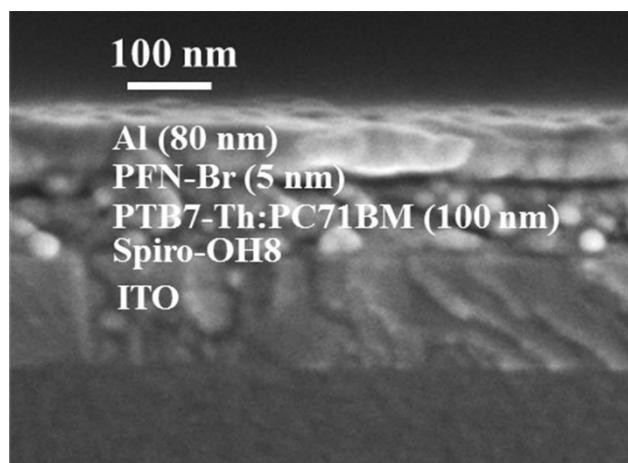


**Figure S24.** The cross-linking SEM image of the PSC device

18. *J-V* and EQE characteristics of devices with different spin-coating concentrations of Spiro-OH8 as HTM

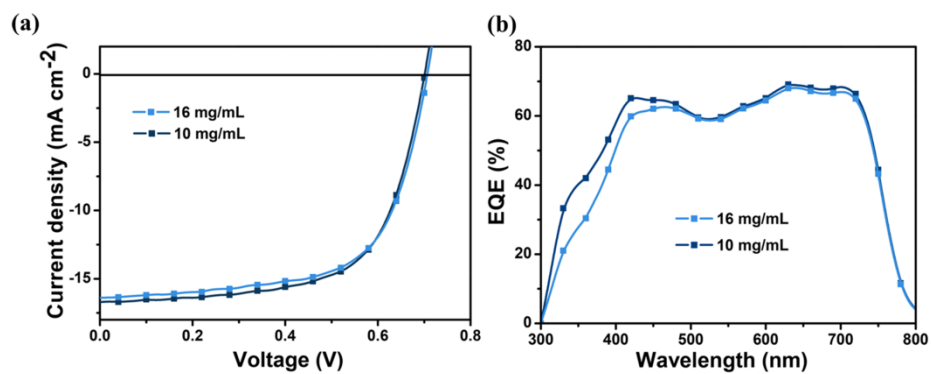


**Figure S25.** *J-V* and EQE characteristics of PSCs devices with different spin-coating concentrations of **Spiro-OH8** (10 mg/mL, 16 mg/mL, respectively) as hole extraction materials.

19. The photovoltaic parameters of Spiro-OH8 based polymer solar cells before and after 216 h storage in nitrogen protected glove box without encapsulation.

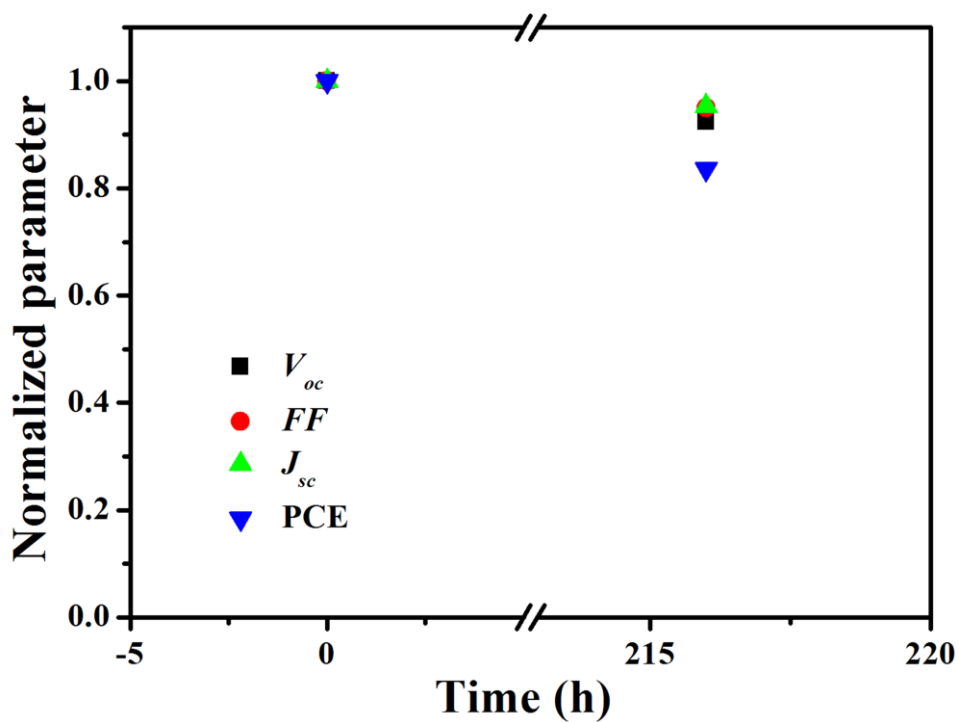


Figure S26. The photovoltaic parameters of Spiro-OH8 based polymer solar cells before and after 216 h storage in nitrogen protected glove box without encapsulation.